Light-induced dynamic RGD pattern for sequential modulation of macrophage phenotypes

Yilun Luo [a], Xiaowen Zheng [a], Peiqi Yuan [a], Xingyao Ye [a], Lie Ma [a,*]

[a] *MOE Key Laboratory of Macromolecular Synthesis and Functionalization, Department of Polymer Science and Engineering, Zhejiang University, Hangzhou, 310027, China*

A R T I C L E   I N F O

A B S T R A C T

Due to the critical roles of macrophage in immune response and tissue repair, harnessing macrophage phenotypes dynamically to match the tissue healing process on demand attracted many attentions. Although there have developed many advanced platforms with dynamic features for cell manipulation, few studies have designed a dynamic chemical pattern to sequentially polarize macrophage phenotypes and meet the immune requirements at various tissue repair stages. Here, we propose a novel strategy for spatiotemporal manipulation of macrophage phenotypes by a UV-induced dynamic Arg-Gly-Asp (RGD) pattern. By employing a photo-patterning technique and the specific interaction between cyclodextrin (CD) and azobenzene-RGD (Azo-RGD), we prepared a polyethylene glycol-dithiol/polyethylene glycol-norbornene (PEG-SH/PEG-Nor) hydrogel with dynamic RGD-patterned surface. After irradiation with 365-nm UV light, the homogeneous RGD surface was transformed to the RGD-patterned surface which induced morphological transformation of macrophages from round to elongated and subsequent phenotypic transition from pro-inflammation to anti-inflammation. The mechanism of phenotypic polarization induced by RGD pattern was proved to be related to Rho-associated protein kinase 2 (ROCK2). Sequential modulation of macrophage phenotypes by the dynamic RGD-patterned surface provides a remote and non-invasive strategy to manipulate immune reactions and achieve optimized healing outcomes.

1. Introduction

Microenvironments of the human body provide dynamic biophysical and biochemical cues that regulate cell fate and organ development [1, 2]. To better understand the dynamic interactions between cells and microenvironments to reveal the intrinsic roles of these regulating cues, advanced platforms with dynamic features, such as surface topography [3], functional ligands [4–6], and stiffness [7–9] have attracted much attention [10,11].

Immune responses play a crucial role in tissue repair and regeneration. Designing biomaterials to precisely regulate immune responses and proactively facilitate tissue repair remains as a significant challenge [12, 13]. As one of the most important innate immune cell types, macrophages with diverse phenotypes direct inflammatory reactions to match the requirements of various repair stages [14,15]. In a normal healing process, at early phase M1 macrophages can activate essential inflammatory response. However, chronic activation of M1 macrophages leads to tissue destruction [16–19] and severe foreign body reaction [20–22],

which is detrimental to hinder tissue repair and regeneration. Therefore, many studies have focused on development of biomaterials with anti-inflammatory properties [23,24]. However, it is widely accepted that the balance of macrophages with pro- and anti-inflammatory phenotypes plays a crucial role in facilitating tissue repair. Therefore, it is necessary to design a platform that dynamically regulates the transition of macrophage phenotypes [25].

Biomaterials with dynamic biochemical or biophysical cues, including cytokines [26–28], adhesion ligands [29], and topography [3, 30] have been designed to sequentially modulate macrophage phenotypes by exogenous stimuli such as magnetic fields [4], near-infrared light [3], and chemical agents [31]. We recently fabricated a "sandwich" cell culture platform with NIR-responsive dynamic stiffness as well to modulate macrophage phenotypes sequentially [9]. However, most strategies are limited to a uniform surface that over-simplifies mimicking the native extracellular matrix (ECM) and does not meet the requirements for microenvironment spatial complexity [2]. We recently demonstrated that NIR-induced microgroove formation on a

---
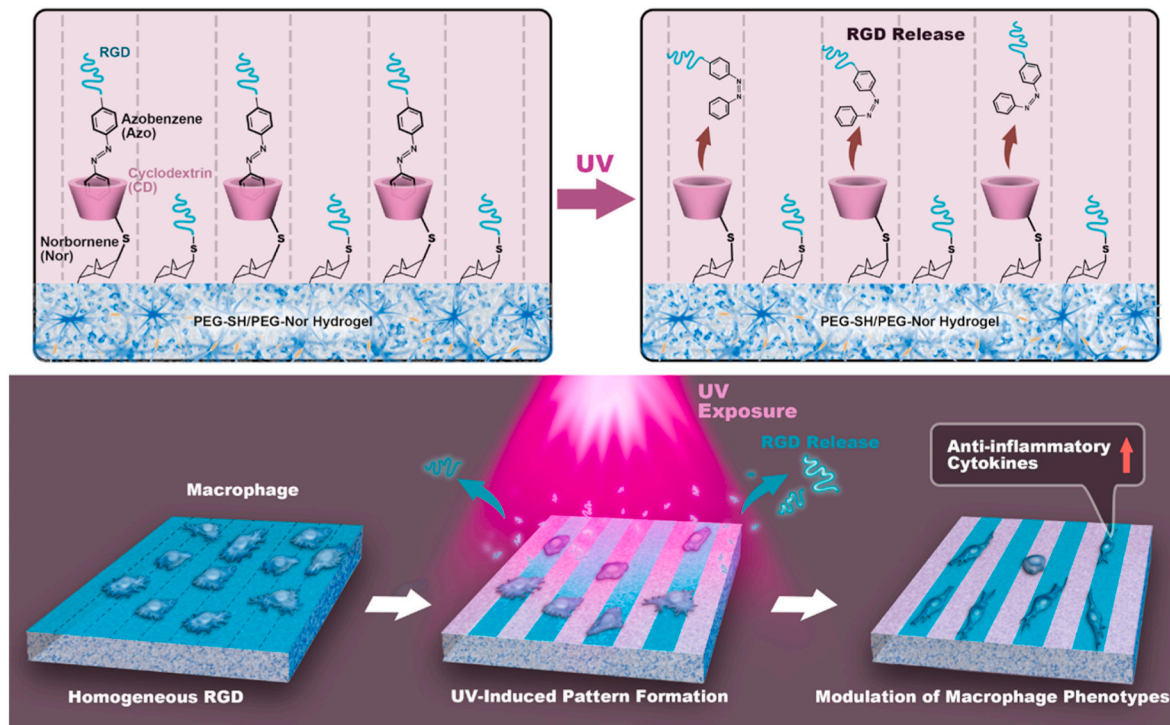
Scheme 1. Schematic of the UV-induced dynamic RGD pattern to sequentially modulate macrophage phenotypes. Under irradiation of 365 nm UV light, the homogeneous RGD surface was transformed to a surface with RGD pattern, which induced morphological transformation of macrophages from round to elongated and subsequent phenotypic transition from pro-inflammation to anti-inflammation.

shape memory film can sequentially modulate macrophages phenotypes from M1 to M2 [3]. Furthermore, compared with a physical microgroove, programmable features of chemical patterns possess excellent ability to mimic the complex native ECM.

Recently, it was demonstrated that a patterned surface induces polarization of macrophages toward the anti-inflammatory phenotype [30, 32–34]. The orientation and alignment of human foreskin fibroblasts were also precisely controlled on micropatterned TiO2 nanodots film [35]. The elongation and polarization of macrophages have been modulated by fibronectin-patterned substrate [32]. Nevertheless, untimely spatial confinement of macrophages by a patterned surface would suppress initiation of the healing process. Therefore, it is important to fabricate a surface with a tunable chemical pattern to dynamically direct the phenotypes of macrophages. Photo-patterning technology that changes the properties of a surface monolith with spatial control has been widely applied to construct patterned surface platforms for cell manipulation [36–39]. However, no study has designed a dynamic chemical pattern to sequentially polarize macrophage phenotypes and meet the immune requirements at various regeneration stages.

Here, we designed a polyethylene glycol (PEG)-based hydrogel substrate with a UV-induced dynamic RGD-patterned surface, which can modulate the morphological transformation and sequential polarization of macrophages on demand to realize a balance of macrophages with pro- and anti-inflammatory phenotypes (Scheme 1). The biocompatible hydrogel substrate was fabricated using eight-arm PEG-norbornene (PEG-Nor) and PEG-dithiol (PEG-SH) through a biorthogonal reaction between the thiol and norbornene groups. By employing a photo-patterning technique and the specific interaction between cyclodextrin (CD) and azobenzene (Azo), we prepared a PEG-based hydrogel substrate with a dynamic RGD-patterned surface. After irradiation with 365-nm UV light, the homogeneous RGD surface was transformed to a surface with patterned RGD, which induced morphological transformation of macrophages from round to elongated and subsequent phenotypic transition from pro-inflammation to anti-inflammation. Sequential modulation of macrophage phenotypes by the dynamic

RGD-patterned surface provides a remote and non-invasive strategy to manipulate immune reactions and achieve optimized healing outcomes.

2. Experimental sections

2.1. Fabrication of the PEG-SH/PEG-Nor hydrogel

Eight-arm PEG norbornene (PEG-Nor) (20000 Da, JenKem Technology, Beijing, China), PEG dithiol (PEG-SH) (3400 Da, eight equiv., Ponsure Biological, Shanghai, China), and 0.05 wt% lithium phenyl (2,4,6-trimethylbenzoyl) phosphinate (LAP, Aladdin, Shanghai, China) were dissolved in phosphate-buffered saline (PBS; 15% w/v). Precursor solutions were passed through a 0.22-μm filter for sterilization. The precursor solution was transferred to a $10 \times 10 \times 0.5 \text{ mm}^3$ silicone mold, covered with olefin-functionalized glass, and irradiated by 365-nm UV light (60 mW/cm^2) for 260 s. The PEG-SH/PEG-Nor hydrogel was removed from the silicon mold and placed in 2 mL PBS for swelling overnight before photopatterning.

2.2. Fabrication of the RGD pattern

The RGD pattern on PEG-SH/PEG-Nor hydrogel surfaces was created via a thiol-ene click reaction between SH-RGD (Cys-Gly-Arg-Gly-Asp-Ser, Top-peptide Biotech, Shanghai, China) and the norbornene group. Fluorescein isothiocyanate-Gly-Gly-Arg-Gly-Asp-Cys (Top-peptide Biotech) was used for pattern visualization. After 50 μL of an RGD/PBS solution (1 mM with 0.05 wt% LAP) was added to the hydrogel, the hydrogel was exposed to UV light (365 nm, Aligner MA6-BSA, Karl Suss, Germany) for 45 s with a photomask, washed with PBS (pH 7.4) more than five times, and then immersed in PBS (pH 7.4) for 6 h.

2.3. Fabrication of the dynamic RGD pattern

Hydrogels with the RGD pattern were coated with a solution of mono-(6-mercapto-6-deoxy)-β-cyclodextrin (SH-β-CD, Zhiyuan Biotech,

Shandong, China) (1 mM with 0.05 wt% LAP), irradiated by UV light (365 nm, 60 mW/cm^2) for 45 s, and then washed as described above. The hydrogels were then placed in a 1 mM azobenzene-Gly-Arg-Gly-Asp-Ser (Azo-GRGDS, Top-peptide Biotech, Shanghai, China) solution for 24 h with gently shaking at 25 °C. Then, the hydrogels were washed with PBS thoroughly and immersed in PBS for 24 h with PBS replacement three times to obtain the hydrogel with the dynamic RGD pattern. Azobenzene-Arg-Gly-Asp-Lys-fluorescein isothiocyanate (Top-peptide Biotech, Shanghai, China) was used for pattern visualization. The pattern on the hydrogels was visualized under a fluorescence microscope (IX81, Olympus, Japan).

2.4. Cell Isolation and culture

C57BL/6 mice (3–5 weeks old, male, Zhejiang Academy of Medical Sciences) were sacrificed to isolate bone marrow-derived macrophages (BMDMs) as reported previously [3] under all relevant ethical regulations after approval by the Animal Ethics Committee of Zhejiang Academy of Medical Sciences. Cells were cultured at 37 °C with 5% CO$_2$ on tissue culture plates in RPMI 1640 medium containing 10% fetal bovine serum (FBS, Gibco, USA). To induce macrophage differentiation, macrophage colony-stimulating factor (20 ng/mL, Novoprotein, Shanghai, China) was added to the medium. The medium was replaced every 2 days. After culture for 3–5 days, BMDMs were collected by trypsinization and seeded on the hydrogels at a density of 100,000 cells/cm^2. To assess the purity of isolated macrophages, BMDMs were labeled with allophycocyanin-conjugated F4/80 (1:50, eBioscience, USA). The corresponding isotype control was used as recommended by the manufacturer.

2.5. Phenotypic analysis of BMDMs

Immunofluorescence staining was used to assess the phenotypic shift of the isolated macrophages. BMDMs were cultured in RPMI 1640 medium containing 10% FBS, 100 ng/mL lipopolysaccharide (LPS, Sigma-Aldrich, China), and 10 ng/mL interferon-γ (IFN-γ, PeproTech, USA) or RPMI 1640 medium containing 10% FBS and 20 ng/mL interleukin-4 (IL-4, R&D Systems, USA) for 12 h. Then, the cells were fixed in methanol for 15 min at 37 °C, permeabilized with 0.5% (v/v) Triton X-100 (Sigma-Aldrich) for 10 min at 4 °C, and then blocked with 3% (w/v) bovine serum albumin (BSA, Beyotime Biotechnology, Hangzhou, China) for 60 min at 37 °C. Cells were stained with a fluorescein isothiocyanate-labeled antibody against inducible nitric oxide synthase (iNOS, 1:50, BD Pharmingen, USA) and PE-labeled antibody against arginase-1 (Arg-1, 1:50, Santa Cruz Biotechnology, USA), washed three times with PBS, and then incubated with DAPI (1:500, Sigma-Aldrich) for 15 min at room temperature. The cells were then imaged under the IX81 fluorescence microscope.

2.6. Cell morphology tracking

BMDMs were seeded on unpatterned (U), patterned (P), or dynamically patterned (D) hydrogels at a density of 100,000 cells/cm^2. After culture for 24 h, the cells were exposed to UV light (365 nm, 50 mW/cm^2) for 60 s and the medium was replaced with fresh RPMI 1640 medium containing 10% FBS. BMDMs were stained with PKH-26 (Sigma-Aldrich, China) in accordance with the manufacturer's instructions and observed at various time points under the fluorescence microscope to track the cell morphological transformation process. Elongation of BMDMs on the hydrogels surfaces was quantitatively analyzed by cellular aspect ratios defined as the longest length divided by the shortest length across the nuclei. Data were analyzed statistically by Image Pro Plus software (Media Cybernetics, USA). More detailed morphologies at several representative time points (8, 16, 24, 32, 40, and 56 h) were further investigated by staining the cytoskeleton and focal adhesions. BMDMs were fixed with 4% paraformaldehyde (PFA)

for 15 min at 37 °C, permeabilized with 0.5% (v/v) Triton X-100 for 10 min at 4 °C, and then blocked with 3% (w/v) BSA for 60 min at 37 °C. Cells were incubated with primary antibodies against vinculin (1:400, R&D Systems) and rhodamine-labeled phalloidin (1:200, Thermo Fisher Scientific, USA) for 12 h at 4 °C. After rinsing in PBS three times, the cells were stained with FITC-labeled goat-anti-mouse IgG (1:2000, Immunoway, China) at room temperature for 2 h and then stained with DAPI (1:1000, Sigma-Aldrich, USA) at room temperature for 15 min. Cells were washed three times with PBS and imaged under a confocal microscope (LSM-510, Zeiss, Germany).

2.7. Analysis of the BMDM phenotype

BMDMs were seeded on unpatterned, patterned, or dynamically patterned hydrogels in a 12-well plate at a density of 100,000 cells/cm^2. After culture for 24 h, the cells were exposed to UV light (365 nm, 50 mW/cm^2) for 60 s, the medium was replaced with fresh RPMI 1640 medium containing 10% FBS, and the cells were cultured for 24 h. BMDM phenotypic transformations were analyzed by immunofluorescence and enzyme-linked immunosorbent assays (ELISAs). Cells with or without UV irradiation were stained for iNOS and Arg-1 as described above. After collecting the culture supernatants of cells, BMDM phenotype-related cytokines, including tumor necrosis factor alpha (TNF-α), interleukin-1β (IL-1β), IL-10, and transforming growth factor-beta (TGF-β1), were analyzed using ELISA kits (Boster, Wuhan, China) in accordance with the manufacturer's instructions.

2.8. Analysis of the phenotypic modulation mechanism

BMDMs were seeded on the hydrogel with dynamic RGD in RPMI 1640 medium containing 10% FBS with or without Y27632 (50 μM, Abcam, Shanghai, China). Cells with or without UV irradiation were stained for iNOS and Arg-1 as described above. Cells were fixed with 4% PFA for 15 min at 37 °C, permeabilized with 0.5% (v/v) Triton X-100 for 10 min at 4 °C, and then blocked with 3% (w/v) BSA for 60 min at 37 °C. Cells were incubated with primary antibodies against ROCK2 (1:150, Abcam) for 12 h at 4 °C. After rinsing in PBS three times, cells were stained with FITC-labeled goat-anti-mouse IgG (1:2000) at room temperature for 2 h and then stained with DAPI (1:1000) at room temperature for 15 min.

2.9. Statistical analysis

At least three independent experiments were carried out to obtain reproducible data if not specifically stated. Data were analyzed with Origin software (MicroCal, USA). Data are expressed as the mean ± standard deviation. Significant differences were assessed by the two-tailed Student's t-test for two groups or one-way ANOVA for three or more groups using SPSS (SPSS Inc., Chicago, IL, USA). A p-value of less than 0.05 was considered statistically significant.

3. Results and discussions

3.1. UV-induced dynamic RGD pattern formation

Because of the effective anti-fouling and biocompatibility of PEG [40], a PEG-based hydrogel was adopted in this study to provide a base substrate that prevented non-specific adhesion of cells. PEG hydrogels modified with RGD in specific areas by photopatterning were fabricated to realize area-selective cell adhesion [41]. To visualize patterned regions, we used RGD-FITC to fabricate patterned hydrogels. Using photomasks with different widths and spacings, we obtained RGD strip patterns with a tunable width and spacing, including a 10-μm width and 10-μm spacing (10/10), 10-μm width and 20-μm spacing (10/20), 20-μm width and 20-μm spacing (20/20), and 20-μm width and 40-μm spacing (20/40) (Fig. S1). β-CD and *trans*-azobenzene spontaneously
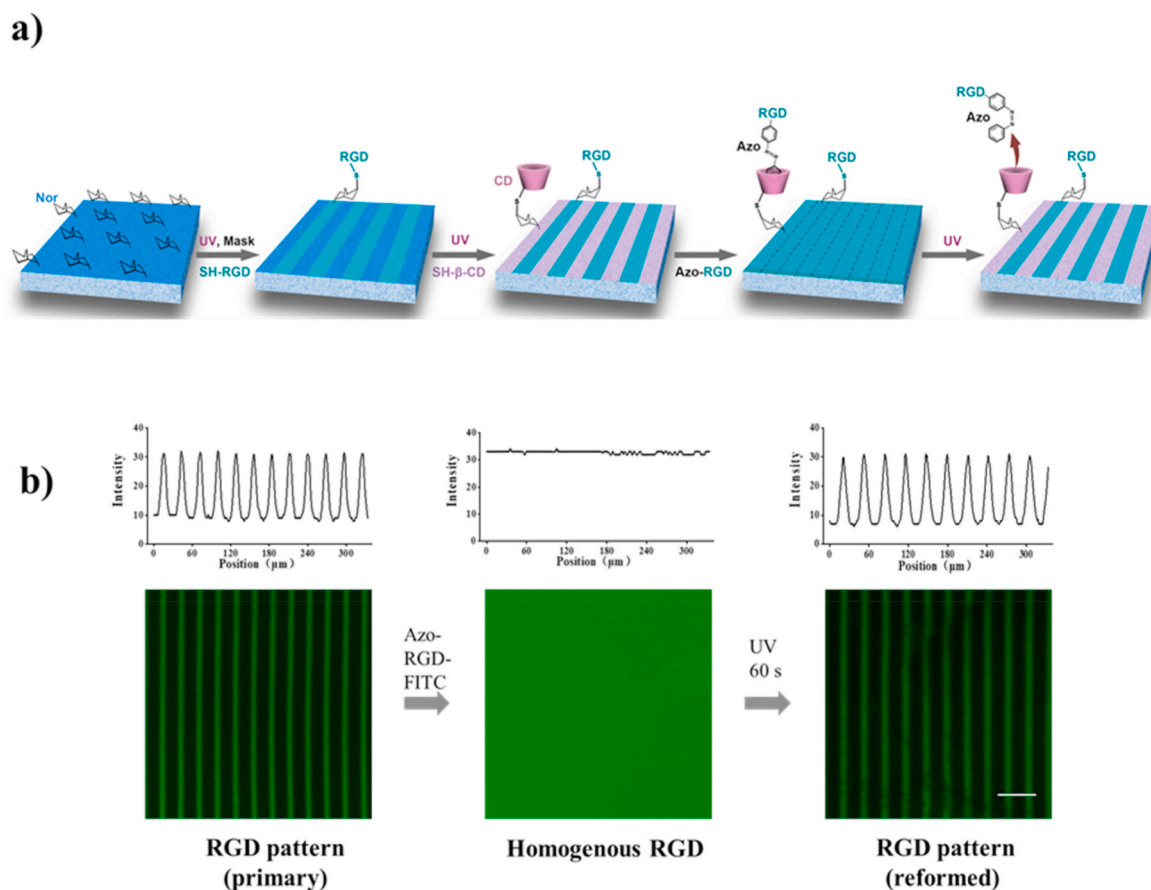
Fig. 1. a) Schematic of the fabrication process of the UV-induced dynamic RGD pattern. b) Fluorescence images and the corresponding intensity profiles of primary RGD pattern, homogenous RGD, and reformed RGD patterns. Scale bar represents 60 μm.

form host-guest complexes. Azobenzene undergoes *trans* to *cis* isomerization under UV irradiation and the size mismatch between *cis*-azobenzene and the β-CD guest disassembles host-guest complexes [42–45]. Photo-switched host-guest system had incomparable superiorities of concise incorporation, convenient control, reversibility, and quick response [46]. UV-triggered disassembly of β-CD and Azo-RGD was used in this study to form the RGD pattern. The UV–vis absorption spectra of Azo-RGD in PBS under irradiation by UV and visible light are shown in Fig. S2. With the increase in UV exposure time, the absorption bands at 325 nm declined remarkably and reached a photo-stationary state after 30 s of irradiation (Fig. S2a). These observations indicated that Azo-RGD underwent UV-triggered disassembly from CD/Azo-RGD complexes and almost complete disassembly was yielded after 30 s of treatment.

The UV-induced dynamic RGD pattern was prepared as described in Fig. 1a. An RGD pattern was fabricated by the thiol-ene click reaction between SH-RGD and surface norbornene groups of PEG-SH/PEG-Nor hydrogel. Then, SH-β-CD was conjugated with double bonds to fill the remaining sites and assembled with Azo-RGD via host-guest recognition. Consequently, a surface with homogeneous RGD was observed. After UV irradiation, the RGD pattern was reformed by release of the assembled Azo-RGD (Fig. 1b). As shown in Fig. S3, being irradiated by UV for 30 s, no clear RGD pattern was formed. When the irradiation time increased to 60 s and more, the surfaces with clear RGD patterns were obtained.

3.2. Morphological transition of BMDMs induced by the dynamic RGD pattern

BMDMs with an F4/80-positive rate of 96.8% were used in the experiment (Fig. S4a) and their phenotypic shift was demonstrated by immunofluorescence staining of iNOS/Arginase-1 (Fig. S4b). After stimulation with 100 ng/mL lipopolysaccharide (LPS) and 10 ng/mL interferon-γ (IFN-γ), BMDMs expressed a high level of iNOS and showed a proinflammatory phenotype. After treatment with 20 ng/mL IL-4, BMDMs expressed a high level of Arg-1, which indicated an anti-inflammatory phenotype. CCK8 assays were performed to evaluate the effect of UV irradiation time on BMDM viability (Fig. S5). With the increase of UV irradiation time, the viabilities of BMDMs were decreased gradually. Considering the effect of UV irradiation time on pattern formation, UV irradiation time of 60 s was adopted to trigger reformation of the RGD pattern and to induce BMDM phenotypic transition in further experiments.

To assess the effect of UV-induced Azo-RGD disassembly on cell adhesion, BMDMs were cultured on an unpatterned hydrogel, that is, a hydrogel with a homogenous RGD surface formed by assembly of β-CD and Azo-RGD. As shown in Fig. S6, modification with β-CD did not affect the anti-adhesion effect of the PEG-based hydrogel. However, with assembly of Azo-RGD, the hydrogel surface showed good promotion of BMDM adhesion. More importantly, BMDMs were efficiently detached from the hydrogel after UV irradiation.

As shown in Fig. S7, PKH-26-stained BMDMs (red) showed a heterogeneous cell distribution on patterned hydrogels. Most BMDMs had adhered to the green strips, that is, the RGD-modified areas. For all patterned hydrogels, the selective adhesion rates were higher than 90%. BMDMs on the 10/20 patterned hydrogel had a higher elongation factor than those on the other hydrogels, which indicated a stronger induction effect on BMDM morphology transition. Immunostaining showed that BMDMs on the 10/20 patterned hydrogel expressed a considerably higher level of Arg-1 but a lower level of iNOS than the other groups, which indicated an anti-inflammatory phenotype (Fig. S8). Therefore,
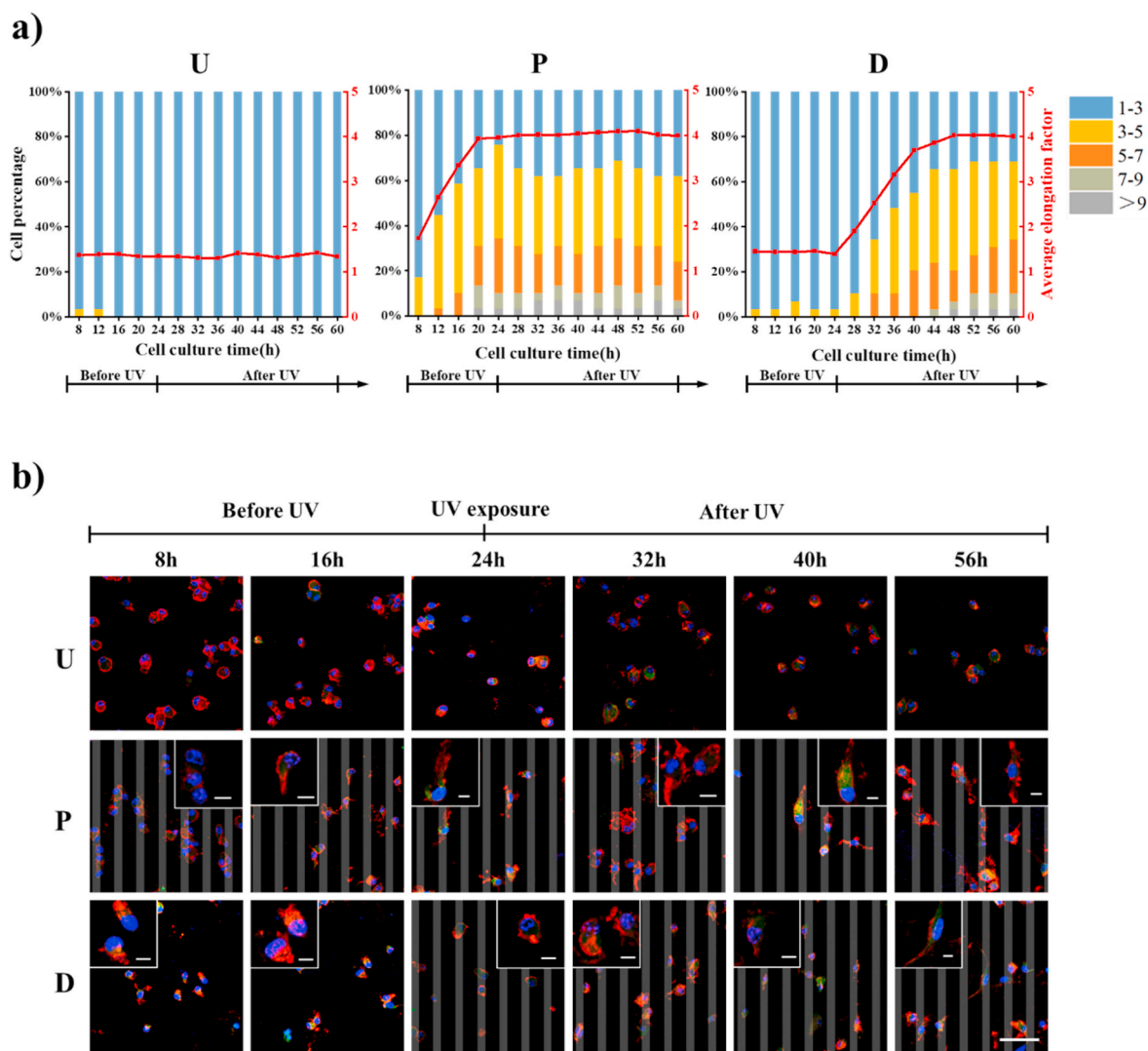
Fig. 2. Dynamic RGD pattern directs elongation of BMDMs. a) Elongation factors of BMDMs cultured on unpatterned (U), patterned (P), and dynamically patterned (D) RGD substrates. The morphologies of BMDMs were observed at several time points by PKH-26 staining under a fluorescence microscope. A minimum of five images were analyzed for each time point. b) CLSM images of BMDMs with immunofluorescence staining of actin (red), vinculin (green), and nuclei (blue). BMDMs were cultured on unpatterned (U), patterned (P), and dynamically patterned (D) RGD substrates for 8, 16, 24, 32, 40, and 56 h. UV irradiation was performed at 24 h. The gray stripe represents the RGD region. Scale bars represent 50 μm and the inset scale bars represent 20 μm.

the hydrogel with the 10/20 pattern was adopted in further experiments.

To track the dynamics of morphological transformation, the elongation factors of BMDMs cultured on unpatterned (U), patterned (P), and dynamically patterned (D) hydrogels were analyzed statistically (Fig. 2a). The results showed that BMDMs on U had a constant and relatively low elongation factor (~1.3) before and after UV irradiation, which indicated no effect of the surface or UV irradiation on cell morphological elongation. Conversely, cells on P elongated immediately, the highest elongation factor of which was obtained after culture for 20 h (approximately 4). No effect of UV irradiation was observed on their elongation factor. BMDMs on D had a similar elongation factor (~1.3) as those on U before UV exposure. After UV exposure, the cells elongated gradually over time and reached the highest elongation (approximately 4) at 48 h.

More detailed morphologies at several representative time points (8, 16, 24, 32, 40, and 56 h) were investigated by staining the cytoskeleton and focal adhesions (Fig. 2b). On U, BMDMs were round and contractile with low vinculin expression. Conversely, macrophages on P had an elongated morphology, predominant actin formation, and increased

vinculin expression. BMDMs cultured on D displayed a round morphology similar to those cultured on U before UV irradiation. After UV irradiation, BMDMs with elongated morphology were observed.

3.3. Sequential regulation of BMDM phenotypes by the dynamic RGD pattern

Immunostaining and ELISAs were used to analyze sequential polarization of BMDMs by the dynamic RGD pattern. The phenotype-related cytokine expression levels of BMDMs on unpatterned and patterned hydrogels were investigated to verify the culture time for effective phenotype transformation. As shown in Fig. S9, the TNF-α level of BMDMs on U was higher than that of BMDMs on P at each time point, but not significant. However, the IL-10 expression level of BMDMs was significantly higher than that of BMDMs on U when the culture time was longer than 24 h, which indicated that RGD pattern-induced phenotypic transformation might require at least 24 h of culture. Therefore, to investigate the sequential polarization effect of the dynamic RGD pattern, BMDMs were precultured on D for 24 h and then further cultured for 24 h after UV exposure for 60 s. BMDMs on D without UV
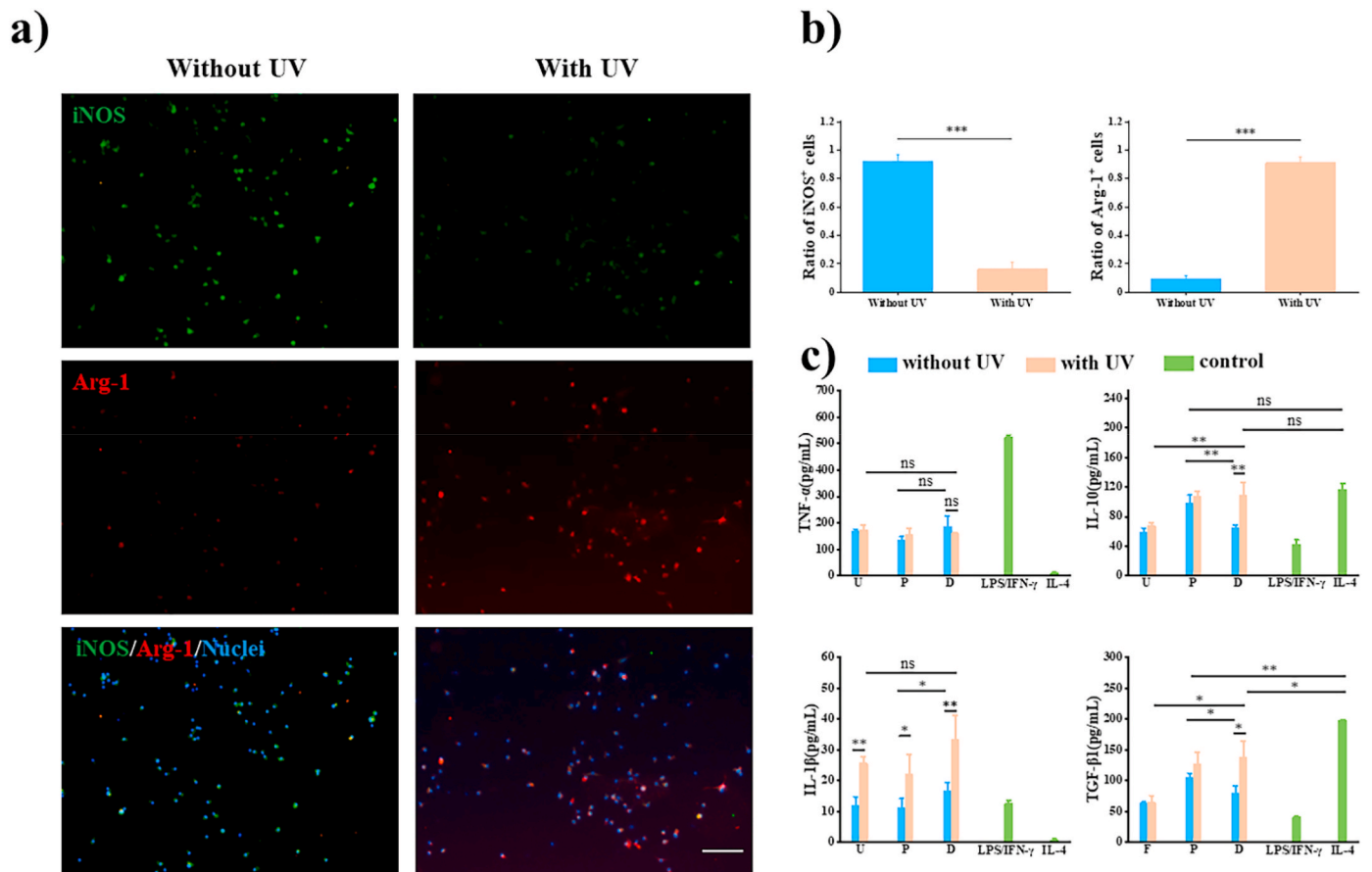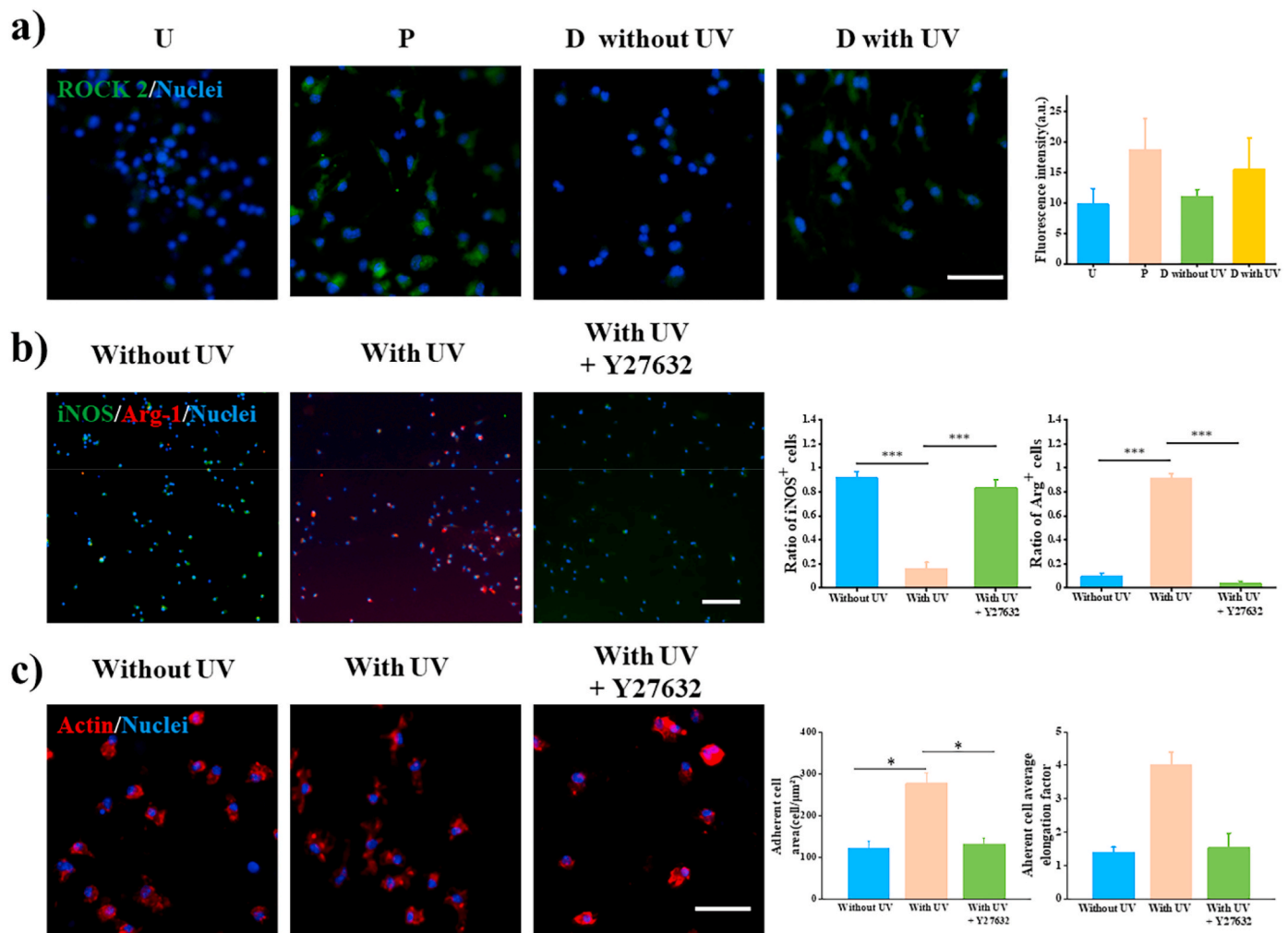
Fig. 3. UV-induced dynamic RGD pattern sequentially regulates BMDM phenotypes. a) Fluorescence images of BMDMs stained for iNOS (green), Arg-1 (red), and nuclei (blue) after culture on the dynamic RGD pattern for 48 h with or without UV irradiation. UV irradiation was performed at 24 h. Scale bar represents 100 μm. b) Corresponding statistical analysis of the numbers of iNOS⁺ or Arg-1⁺ cells. c) Corresponding secreted levels of TNF-α, IL-1β, IL-10, and TGF-β1 determined by ELISAs. All experiments were carried out at least three times independently and analyzed using Origin software (MicroCal, USA). Data are expressed as the mean ± standard deviation. Significant differences were assessed by the two-tailed Student's t-test for two groups or one-way ANOVA for three or more groups using SPSS (SPSS Inc., Chicago, IL, USA). $*p < 0.05$, $**p < 0.01$, $***p < 0.001$.

irradiation were used as the control. iNOS and Arg-1 expression in BMDMs cultured on D before and after UV irradiation was investigated by immunostaining (Fig. 3a). The numbers of iNOS⁺ and Arg-1⁺ cells with and without UV irradiation were statistically analyzed using Image Pro Plus (Fig. 3b). There were more iNOS⁺ cells observed on D without UV exposure. Conversely, more Arg-1⁺ cells were observed after UV exposure. The phenotypes of BMDMs were further analyzed by ELISAs (Fig. 3c). After stimulation with LPS/IFN-γ, BMDMs expressed high levels of TNF-α and IL-1β, which were the control for M1 macrophages. IL-4-treated macrophages with high levels of IL-10 and TGF-β1 were used as the control for M2 macrophages [47]. As shown in Fig. 3c, there was no significant difference in TNF-α expression regardless of the hydrogel substrate and UV exposure. However, IL-1β expression of BMDMs on U, P, and D was increased by UV irradiation. Furthermore, with or without UV exposure, there were no significant differences in TNF-α, IL-10, or TGF-β1 expression on U except for IL-1β. Anti-inflammatory cytokine IL-10 expression was enhanced on P, similar to that of the M2 control. Fig. S8 shows that macrophages on P expressed a high level of Arg-1, which confirmed that the chemical pattern promoted a shift in phenotype. Without UV irradiation, macrophages on U and D secreted similarly low levels of IL-10, whereas UV-irradiated macrophages on D expressed significantly higher levels of IL-10 and were similar to the M2 control. Interestingly, Arg⁺IL-10^hiTGF-β1^hi MΦ and M2a (a subtype of M2 macrophages) shared a similar upregulation of IL-10, TGF-β1, and Arg-1, and M2a has been demonstrated to be essential in the proliferative phase of wound healing [25,48,49]. These

findings supported that the UV-induced dynamic pattern formation modulated macrophage polarization from M1 to M2. Traditionally defined classical M1 and M2 macrophages are induced by cytokines. However, the bipolar definition is oversimplified and there are no distinct categories between M1 and M2 types [50]. Many additional subtypes of macrophages have been defined in some studies [25]. Therefore, polarization degrees of M1- or M2-like qualities should be different under chemical and physical stimulations. Consequently, pattern induction might not be exactly the same as cytokine induction.

3.4. Investigation of the phenotypic modulation mechanism

To explore the mechanism of phenotypic polarization induced by the chemical pattern, macrophages were stained for Rho-associated protein kinase 2 (ROCK2) [51,52]. ROCK is a crucial regulator of actin cytoskeletal organization and cell-adhesive junctions. The ROCK2 isoform mediates polarization of macrophages, which is considered a molecular switch of macrophage polarization [6,29,53]. As shown in Fig. 4a, BMDMs on P and D with UV irradiation expressed significantly high levels of ROCK2. While, the results in Fig. 4b shows that BMDMs on D with UV irradiation and Y27632 (a ROCK inhibitor) ROCK inhibition expressed higher iNOS levels and lower Arg-1 levels compared with those on D with UV irradiation. Moreover, the cytoskeletal construction of BMDMs was also investigated (Fig. 4b). Notably, BMDMs on D with UV irradiation and ROCK inhibition had a reduced adherent cell area and elongation (Fig. 4c). In summary, these findings illustrated that

Fig. 4. Dynamic RGD pattern-regulated phenotypic transition of BMDMs is related to high expression levels of the cytoskeleton-related signal ROCK. a) Immuno-fluorescence images of BMDMs stained for ROCK2 (green) and nuclei (blue) after culture on unpatterned (U), patterned (P), and dynamically patterned (D) RGD substrates for 48 h with or without UV irradiation. UV irradiation was performed at 24 h. Scale bar represents 50 μm. b) Fluorescence images and corresponding statistical results of BMDMs immunostained for iNOS (green), Arg-1 (red), and nuclei (blue). Scale bar represents 100 μm. c) Fluorescence images of BMDMs immunostained for actin (red) and nuclei (blue), and the corresponding statistical results of the adhesion area and elongation factor of BMDMs. Cells were cultured on the dynamic RGD pattern for 24 h with or without UV irradiation. UV irradiation was performed at 16 h. BMDMs under UV irradiation were also treated with ROCK inhibitor Y27632. Scale bar represents 50 μm $*p < 0.05$, $**p < 0.01$, $***p < 0.001$ (two-tailed Student's t-test).

modulation of macrophage adhesion and polarization by the RGD pattern was related to ROCK2.

4. Conclusions

We fabricated the PEG-based hydrogels with UV-induced dynamic RGD-pattern. Under UV exposure, Azo-RGD was isomerized and released from β-CD, which rapidly converted the homogeneous surface to an RGD-patterned surface. Subsequently, macrophages detached from non-adhesive regions, adhered on the adhesive regions, and elongated along the RGD pattern. The RGD pattern induced a morphological shift of macrophages from round to elongated and modulated phenotypic transformation. The elongation factor of macrophages before UV irradiation was maintained at 1.3 and increased sharply to about 4 after UV irradiation. The morphological transformation converted macrophages from iNOS$^+$IL-10^{lo} (pro-inflammation) to Arg-1$^+$IL-10^{hi} (anti-inflammation) and influence ROCK2 signaling. The precise spatiotemporal manipulation of macrophage phenotypes induced by the dynamic RGD pattern offers a novel strategy to promote regenerative immune processes and provides a new platform for immunomodulatory biomaterials.

CRediT authorship contribution statement

Yilun Luo: Conceptualization, Methodology, Investigation, Data curation, Writing – original draft. **Xiaowen Zheng:** Conceptualization, Methodology. **Peiqi Yuan:** Methodology, Investigation. **Xingyao Ye:** Methodology. **Lie Ma:** Conceptualization, Supervision, Writing – review & editing, Funding acquisition.

Declaration of competing interest

The authors declare that they have no known competing financial interests or personal relationships that could have appeared to influence the work reported in this paper.

Appendix A. Supplementary data

Supplementary data to this article can be found online at https://doi.org/10.1016/j.bioactmat.2021.04.018.

References

[1] K. Uto, J.H. Tsui, C.A. DeForest, D.H. Kim, Dynamically tunable cell culture platforms for tissue engineering and mechanobiology, Prog. Polym. Sci. 65 (2017) 53–82.

[2] J.A. Shadish, G.M. Benuska, C.A. DeForest, Bioactive site-specifically modified proteins for 4D patterning of gel biomaterials, Nat. Mater. 18 (9) (2019) 1005–1014.

[3] X. Zheng, L. Xin, Y. Luo, H. Yang, X. Ye, Z. Mao, S. Zhang, L. Ma, C. Gao, Near-infrared-triggered dynamic surface topography for sequential modulation of macrophage phenotypes, ACS Appl. Mater. Interfaces 11 (2019) 43689–43697.

[4] H. Kang, S. Kim, D.S.H. Wong, H.J. Jung, S. Lin, K. Zou, R. Li, G. Li, V.P. David, L. Bian, Remote manipulation of ligand nano-oscillations regulates adhesion and polarization of macrophages in vivo, Nano Lett. 17 (2017) 6415–6427.

[5] H. Kang, K. Zhang, H.J. Jung, B. Yang, X. Chen, Q. Pan, R. Li, X. Xu, G. Li, V.P. David, L. Bian, An in situ reversible heterodimeric nanoswitch controlled by metal-ion-ligand coordination regulates the mechanosensing and differentiation of stem cells, Adv. Mater. 30 (2018) 1803591.

[6] S. Min, Y.S. Jeon, H. Choi, C. Khatua, N. Li, G. Bae, H.J. Jung, Y. Kim, H. Hong, J. Shin, M.J. Ko, H.S. Ko, T. Kim, J.H. Moon, J.J. Song, V.P. Dravid, Y.K. Kim, H. Kang, Large and externally positioned ligand-coated nanopatches facilitate the adhesion-dependent regenerative polarization of host macrophages, Nano Lett. 20 (2020) 7272–7280.

[7] K.A. Kyburz, K.S. Anseth, Synthetic mimics of the extracellular matrix: how simple is complex enough? Ann. Biomed. Eng. 43 (3) (2015) 489–500.

[8] Z. Zhuang, Y. Zhang, S. Sun, Q. Li, K. Chen, C. An, L. Wang, J. van den Beucken, H. Wang, Control of matrix stiffness using methacrylate-gelatin hydrogels for a macrophage-mediated inflammatory response, ACS Biomater. Sci. Eng. 6 (5) (2020) 3091–3102.

[9] P. Yuan, Y. Luo, Y. Luo, L. Ma, A "sandwich" cell culture platform with NIR-responsive dynamic stiffness to modulate macrophage phenotypes, Biomater. Sci. (2021), https://doi.org/10.1039/d0bm02194f.

[10] D.S. Hernandez, E.T. Ritschdorff, J.L. Connell, J.B. Shear, In situ imprinting of topographic landscapes at the cell-substrate interface, J. Am. Chem. Soc. 140 (43) (2018) 14064–14068.

[11] L.C. Bahlmann, A. Fokina, M.S. Shoichet, Dynamic bioengineered hydrogels as scaffolds for advanced stem cell and organoid culture, MRS Commun 7 (3) (2017) 472–486.

[12] Z. Julier, A.J. Park, P.S. Briquez, M.M. Martino, Promoting tissue regeneration by modulating the immune system, Acta Biomater. 53 (2017) 13–28.

[13] A.K. Gaharwar, I. Singh, A. Khademhosseini, Engineered biomaterials for in situ tissue regeneration, Nat. Rev. Mater. 5 (2020) 686–705.

[14] K.L. Spiller, T.J. Koh, Macrophage-based therapeutic strategies in regenerative medicine, Adv. Drug Deliv. Rev. 122 (2017) 74–83.

[15] C.E. Witherel, D. Abebayehu, T.H. Barker, K.L. Spiller, Macrophage and fibroblast interactions in biomaterial-mediated fibrosis, Adv. Healthcare Mater. 8 (4) (2019) 1801451.

[16] T.D. Smith, R.R. Nagalla, E.Y. Chen, W.F. Liu, Harnessing macrophage plasticity for tissue regeneration, Adv. Drug Deliv. Rev. 114 (2017) 193–205.

[17] E.M. O'Brien, G.E. Risser, K.L. Spiller, Sequential drug delivery to modulate macrophage behavior and enhance implant integration, Adv. Drug Deliv. Rev. 149–150 (2019) 85–94.

[18] G. Zhou, T. Groth, Host responses to biomaterials and anti-inflammatory design-a brief review, Macromol. Biosci. 18 (8) (2018) 1800112.

[19] Y.K. Kim, E.Y. Chen, W.F. Liu, Biomolecular strategies to modulate the macrophage response to implanted materials, J. Mater. Chem. B 4 (9) (2016) 1600–1609.

[20] J. Li, X. Jiang, H. Li, M. Gelinsky, Z. Gu, Tailoring materials for modulation of macrophage fate, Adv. Mater. (2021), e2004172.

[21] J.M. Anderson, A. Rodriguez, D.T. Chang, Foreign body reaction to biomaterials, Semin. Immunol. 20 (2) (2008) 86–100.

[22] A. Vishwakarma, N.S. Bhise, M.B. Evangelista, J. Rouwkema, M.R. Dokmeci, A.M. Ghaemmaghami, N.E. Vrana, A. Khademhosseini, Engineering immunomodulatory biomaterials to tune the inflammatory response, Trends Biotechnol. 34 (6) (2016) 470–482.

[23] V. Riabov, F. Salazar, S.S. Htwe, A. Gudima, C. Schmuttermaier, J. Barthes, H. Knopf-Marques, H. Kluter, A.M. Ghaemmaghami, N.E. Vrana, J. Kzhyshkowska, Generation of anti-inflammatory macrophages for implants and regenerative medicine using self-standing release systems with a phenotype-fixing cytokine cocktail formulation, Acta Biomater. 53 (2017) 389–398.

[24] C. Chu, L. Liu, Y. Wang, R. Yang, C. Hu, S. Rung, Y. Man, Y. Qu, Evaluation of epigallocatechin-3-gallate (EGCG)-modified scaffold determines macrophage recruitment, Mater. Sci. Eng. C Mater. Biol. Appl. 100 (2019) 505–513.

[25] P. Krzyszczyk, R. Schloss, A. Palmer, F. Berthiaume, The role of macrophages in acute and chronic wound healing and interventions to promote pro-wound healing phenotypes, Front. Physiol. 9 (2018) 419.

[26] K.L. Spiller, S. Nassiri, C.E. Witherel, R.R. Anfang, J. Ng, K.R. Nakazawa, T. Yu, G. Vunjak-Novakovic, Sequential delivery of immunomodulatory cytokines to facilitate the M1-to-M2 transition of macrophages and enhance vascularization of bone scaffolds, Biomaterials 37 (2015) 194–207.

[27] M.M. Alvarez, J.C. Liu, G. Trujillo-de Santiago, B.H. Cha, A. Vishwakarma, A.M. Ghaemmaghami, A. Khademhosseini, Delivery strategies to control inflammatory response: modulating M1-M2 polarization in tissue engineering applications, J. Contr. Release 240 (2016) 349–363.

[28] C. Chu, L. Liu, Y. Wang, S. Wei, Y. Wang, Y. Man, Y. Qu, Macrophage phenotype in the epigallocatechin-3-gallate (EGCG)-modified collagen determines foreign body reaction, J Tissue Eng. Regen. Med. 12 (6) (2018) 1499–1507.

[29] H. Kang, S.H.D. Wong, Q. Pan, G. Li, L. Bian, Anisotropic ligand nanogeometry modulates the adhesion and polarization state of macrophages, Nano Lett. 19 (3) (2019) 1963–1975.

[30] M.J. Vassey, G.P. Figueredo, D.J. Scurr, A.S. Vasilevich, S. Vermeulen, A. Carlier, J. Luckett, N.R.M. Beijer, P. Williams, D.A. Winkler, J. de Boer, A.M. Ghaemmaghami, M.R. Alexander, Immune modulation by design: using topography to control human monocyte attachment and macrophage differentiation, Adv. Sci. 7 (11) (2020) 1903392.

[31] H. Kang, B. Yang, K. Zhang, Q. Pan, W. Yuan, G. Li, L. Bian, Immunoregulation of macrophages by dynamic ligand presentation via ligand-cation coordination, Nat. Commun. 10 (1) (2019) 1696.

[32] F.Y. McWhorter, T. Wang, P. Nguyen, T. Chung, W.F. Liu, Modulation of macrophage phenotype by cell shape, Proc. Natl. Acad. Sci. 110 (43) (2013) 17253–17258.

[33] T.U. Luu, S.C. Gott, B.W. Woo, M.P. Rao, W.F. Liu, Micro- and nanopatterned topographical cues for regulating macrophage cell shape and phenotype, ACS Appl. Mater. Interfaces 7 (51) (2015) 28665–28672.

[34] N. Jain, V. Vogel, Spatial confinement downsizes the inflammatory response of macrophages, Nat. Mater. 17 (12) (2018) 1134–1144.

[35] C. Liu, Y. Zhou, M. Sun, Q. Li, L. Dong, L. Ma, K. Cheng, W. Weng, M. Yu, H. Wang, Light-induced cell alignment and harvest for anisotropic cell sheet technology, ACS Appl. Mater. Interfaces 9 (42) (2017) 36513–36524.

[36] W.M. Gramlich, I.L. Kim, J.A. Burdick, Synthesis and orthogonal photopatterning of hyaluronic acid hydrogels with thiol-norbornene chemistry, Biomaterials 34 (38) (2013) 9803–9811.

[37] J.C. Grim, T.E. Brown, B.A. Aguado, D.A. Chapnick, A.L. Viert, X. Liu, K.S. Anseth, A reversible and repeatable thiol-ene bioconjugation for dynamic patterning of signaling proteins in hydrogels, ACS Cent. Sci. 4 (7) (2018) 909–916.

[38] R.J. Wade, E.J. Bassin, W.M. Gramlich, J.A. Burdick, Nanofibrous hydrogels with spatially patterned biochemical signals to control cell behavior, Adv. Mater. 27 (8) (2015) 1356.

[39] K.A. Mosiewicz, L. Kolb, A.J. van der Vlies, M.M. Martino, P.S. Lienemann, J.A. Hubbell, M. Ehrbar, M.P. Lutolf, In situ cell manipulation through enzymatic hydrogel photopatterning, Nat. Mater. 12 (11) (2013) 1072–1078.

[40] B.K.D. Ngo, M.A. Grunlan, Protein resistant polymeric biomaterials, ACS Macro Lett. 6 (9) (2017) 992–1000.

[41] C. Chu, J. Deng, Y. Hou, L. Xiang, Y. Wu, Y. Qu, Y. Man, Application of PEG and EGCG modified collagen-base membrane to promote osteoblasts proliferation, Mater. Sci. Eng. C Mater. Biol. Appl. 76 (2017) 31–36.

[42] B.V.K.J. Schmidt, C. Barner-Kowollik, Dynamic macromolecular material design-the versatility of cyclodextrin-based host-guest chemistry, Angew. Chem. Int. Ed. 56 (29) (2017) 8350–8369.

[43] D. Wang, F. Schellenberger, J.T. Pham, H.J. Butt, S. Wu, Orthogonal photo-switching of supramolecular patterned surfaces, Chem. Commun. 54 (27) (2018) 3403–3406.

[44] Y.-H. Gong, C. Li, J. Yang, H.-Y. Wang, R.-X. Zhuo, X.-Z. Zhang, Photoresponsive "smart template" via host–guest interaction for reversible cell adhesion, Macromolecules 44 (19) (2011) 7499–7502.

[45] J. Liu, H.J. Butt, S. Wu, Reconfigurable surfaces based on photocontrolled dynamic bonds, Adv. Funct. Mater. 30 (26) (2019).

[46] Q. Bian, W. Wang, G. Wang, Light-triggered specific cancer cell release from cyclodextrin/azobenzene and aptamer-modified substrate, ACS Appl. Mater. Interfaces 8 (40) (2016) 27360–27367.

[47] D.M. Mosser, J.P. Edwards, Exploring the full spectrum of macrophage activation, Nat. Rev. Immunol. 8 (12) (2008) 958–969.

[48] C. Chu, J. Deng, X. Sun, Y. Qu, Y. Man, Collagen membrane and immune response in guided bone regeneration: recent progress and perspectives, Tissue Eng. B Rev. 23 (5) (2017) 421–435.

[49] C. Chu, L. Liu, S. Rung, Y. Wang, Y. Ma, C. Hu, X. Zhao, Y. Man, Y. Qu, Modulation of foreign body reaction and macrophage phenotypes concerning microenvironment, J. Biomed. Mater. Res. 108 (1) (2020) 127–135.

[50] F.O. Martinez, S. Gordon, The M1 and M2 paradigm of macrophage activation: time for reassessment, F1000Prime Rep. 6 (2014) 13.

[51] G.R. John, Interleukin-1 induces a reactive astroglial phenotype via deactivation of the Rho GTPase-rock Axis, J. Neurosci. 24 (11) (2004) 2837–2845.

[52] E. Gruber, C. Heyward, J. Cameron, C. Leifer, Toll-like receptor signaling in macrophages is regulated by extracellular substrate stiffness and Rho-associated coiled-coil kinase (ROCK1/2), Int. Immunol. 30 (6) (2018) 267–278.

[53] S. Zandi, S. Nakao, K.H. Chun, P. Fiorina, D. Sun, R. Arita, M. Zhao, E. Kim, O. Schueller, S. Campbell, M. Taher, M.I. Melhorn, A. Schering, F. Gatti, S. Tezza, F. Xie, A. Vergani, S. Yoshida, K. Ishikawa, M. Yamaguchi, F. Sasaki, R. Schmidt-Ullrich, Y. Hata, H. Enaida, M. Yuzawa, T. Yokomizo, Y.B. Kim, P. Sweetnam, T. Ishibashi, A. Hafezi-Moghadam, ROCK-isoform-specific polarization of macrophages associated with age-related macular degeneration, Cell Rep. 10 (7) (2015) 1173–1186.